Stanford Exploration Project, Report 120, May 3, 2005, pages 365–377

Water-bottom and diffracted 2D multiple reflections in data space and image space

Gabriel Alvarez[1]

ABSTRACT

Water-bottom multiples from a dipping interface have the same kinematics in a Common Midpoint (CMP) gather as a primary from a reflector with twice the dip at twice the perpendicular depth at the CMP location. When migrated with the velocity of the primaries, these multiples are overmigrated just as primaries migrated with higher velocity, and their moveout is thus predictable in image space. Diffracted multiples, on the other hand, have an apex-shifted moveout in CMP gathers and a more complicated, also apex-shifted, residual moveout in image space when migrated with the velocity of the primaries. I illustrate the moveout of water-bottom and diffracted multiples in image space with a simple 2D synthetic dataset.

INTRODUCTION

Recently, the increased interest in exploration in areas with rough salt bodies, such as the Gulf of Mexico, has sparkled the interest in multiple attenuation methods that work in the image space (Sava and Guitton, 2003; Hargreaves and Wombell, 2004; Alvarez et al., 2004) as opposed to more traditional methods that work in the data space (Hampson, 1986) or Surface Related Multiple Elimination (SRME) methods (Verschuur et al., 1992; Verschuur and Berkhout, 1997) that require dense surface coverage of sources and receivers or demanding data interpolation and extrapolation.

The main advantage of the image space is that most of the complexity of the propagation for the primary reflections is handled by prestack depth migration such that the primary reflections in Angle-Domain Common-Image Gathers (ADCIGs) are flat or nearly flat if the migration is done with the velocity of the primaries. It is not immediately obvious, however, what is the residual moveout of the migrated multiples in ADCIGs. A reasonable approximation is to consider that the residual moveout of the migrated multiples is the same as that of the primaries when migrated with the wrong (higher) velocity (Biondi and Symes, 2004). This approach leads, in 2D, to a relatively simple and effective algorithm for the attenuation of the multiples in the image space (Sava and Guitton, 2003) and, with some modifications, can

[1]**email:** gabriel@sep.stanford.edu

attenuate 2D diffracted multiples reasonably well (Alvarez et al., 2004). In this paper I present the equations for the image space coordinates of the water-bottom multiples in 2D ADCIGs and illustrate the migration of the multiples with a synthetic dataset.

The next section presents the kinematics of water-bottom and diffracted multiples in data space. The following section presents the equations to map the multiples from data space to image space. The last section illustrates the mapping of the multiples in image space, both in common subsurface offset common-image gathers and angle-domain common-image gathers for the simple synthetic dataset.

KINEMATICS OF MULTIPLES IN DATA SPACE FROM A 2D DIPPING INTERFACE

Water-bottom multiples

Consider a model with a dipping water-bottom in 2D. The raypath of the primary reflection can be easily computed using the concept of the image source as illustrated in Figure 1. The

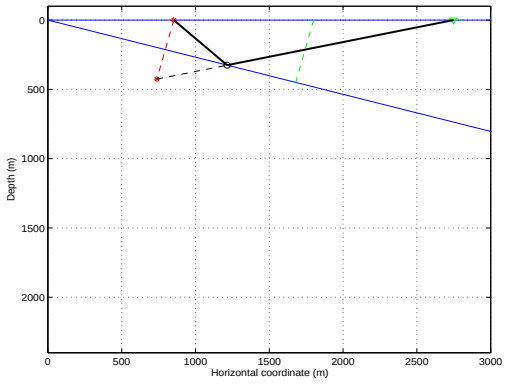

Figure 1: Construction of the primary reflection from a dipping interface. gabriel2-rayprim [CR]

moveout of the primary reflection in the CMP domain is given by:

$$t_p = \sqrt{\left(\frac{2Z_D}{V}\right)^2 + \left(\frac{2h_D}{V_{NMO}}\right)^2} = \sqrt{t_0^2 + \left(\frac{2h_D}{V_{NMO}}\right)^2} \tag{1}$$

where t_p is the time of the primary, φ is the dip angle of the reflector, Z_D is the perpendicular distance between the surface and the reflector at the CMP location, h_D is half the source-receiver offset, V is the propagation velocity above the dipping reflector, $V_{NMO} = V/\cos\varphi$ is the normal moveout velocity and t_0 is the traveltime of the zero-offset reflection. This is obviously the equation of a hyperbola, as illustrated in Figure 4.

The raypath of the multiple reflection can be considered as a cascaded of two primary reflections as SRME methods do (Figure 2), but the traveltime of the multiple, t_m, can be computed more easily as the traveltime of an equivalent primary from a reflector dipping at

twice the dip angle of the actual reflector as illustrated in Figure 3. That is,

$$t_m = \sqrt{\left(\frac{2\hat{Z}_D}{V}\right)^2 + \left(\frac{2h_D}{\hat{V}_{NMO}}\right)^2} \tag{2}$$

where $\hat{Z}_D$ is the perpendicular distance between the surface and the equivalent reflector with twice the dip at the CMP location and $\hat{V}_{NMO}$ is now $V/\cos(2\varphi)$. Figure 4 corresponds to a CMP showing the primary and the multiple reflection. Obviously, they are both hyperbolas since the multiple has the same kinematics as a primary from a reflector dipping at twice the dip as indicated above.

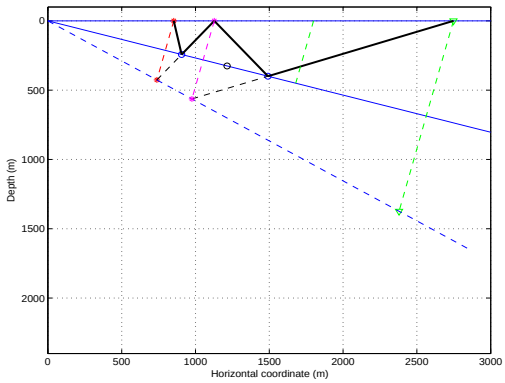

Figure 2: Decomposition of the water-bottom multiple as a cascaded of two primary reflections. gabriel2-raymul1 [CR]

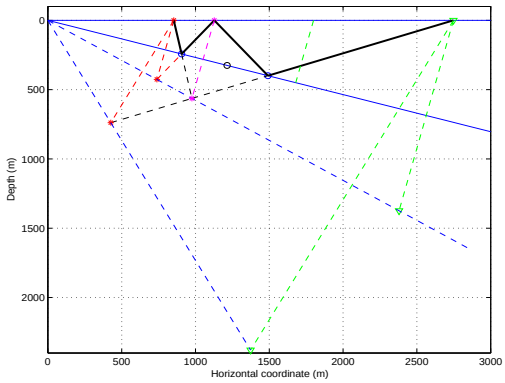

Figure 3: Multiple reflection as a primary from an equivalent reflector with twice the dip angle. gabriel2-raymul2 [CR]

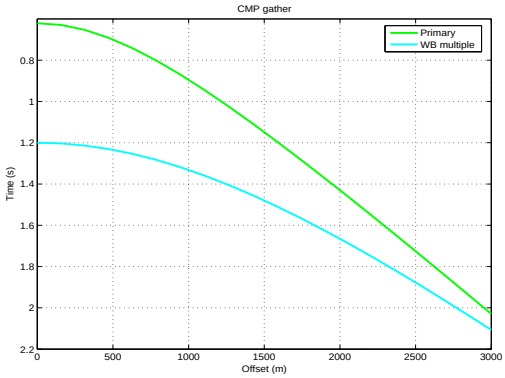

Figure 4: Moveout curves of primary and water-bottom multiple from a dipping interface on a CMP gather. gabriel2-moveouts1 [CR]

Diffracted multiples

Consider now a diffractor sitting on top of the water-bottom reflector at the lateral position x_d and depth z_d (Figure 5). The moveout of the primary diffraction is given by

$$t_d = t_s + t_g = \frac{1}{V}\left[\sqrt{(x_d - m_D + h_D)^2 + z_d^2} + \sqrt{(m_D + h_D - x_d)^2 + x_d^2}\right] \tag{3}$$

where t_s and t_g are traveltimes from the source and receiver to the diffractor, respectively, m_D is the horizontal position of the CMP gather and h_D is the half-offset between the source and the receiver. This is the equation of a hyperbola with apex at the horizontal position directly above the diffractor. Consider now the multiple that hits the diffractor on its second bounce on

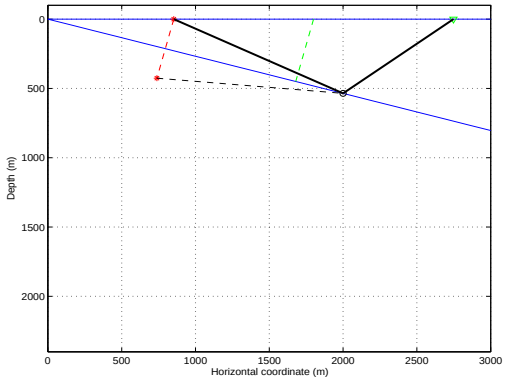

Figure 5: Image source construction for the primary diffraction. gabriel2-rayprimdiff [CR]

the dipping reflector (source-side multiple), as shown in Figure 6. This multiple is no longer the equivalent of any primary, but we can compute its traveltime in the following way:

1. Form the image source.
2. Find the point at the surface such that the lines joining that point with both the image source and the diffractor intercept with the same angle with respect to the vertical (Snell's law).
3. Compute the raypath using the law of cosines and divide by the velocity to get the traveltime.

The coordinates of the image source (X_{is}, Z_{is}) are given by

$$X_{is} = X_s - 2Z_0 \sin\varphi, \tag{4}$$
$$Z_{is} = 2Z_0 \cos\varphi, \tag{5}$$

where

$$Z_0 = Z_D - h_D \sin\varphi \tag{6}$$

is the perpendicular distance between the shot and the reflector. From the description of nu-

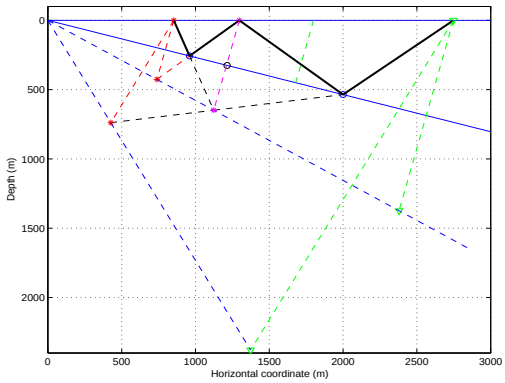

Figure 6: Diffracted multiple. Notice that the last leg of the multiple does not satisfy Snell's law. gabriel2-raymuldiff [CR]

meral 3. above, the surface coordinate of the multiple bounce at the surface is:

$$X_{ms} = \frac{X_{is} z_d + x_d Z_{is}}{Z_{is} + z_d}. \tag{7}$$

The aperture angle of the first bounce of the multiple is $\beta_s + \varphi$ where β_s is the takeoff angle of the multiple with respect to the vertical. The aperture angle at the surface bounce is $\beta_s + 2\varphi$ and can be easily computed as

$$\tan(\beta_s + 2\varphi) = \frac{x_d - X_{ms}}{z_d}. \tag{8}$$

The traveltime of the first leg of the multiple, in terms of β_s and the vertical distance between the source and the reflector, $Z_s = \frac{Z_D - h_D \sin\varphi}{\cos\varphi}$, is:

$$t_{m_1} = \frac{Z_s \cos\varphi}{V \cos(\varphi + \beta_s)}. \tag{9}$$

Similarly, repeated application of the law of sines gives the traveltime of the other three legs of the multiple

$$t_{m_2} = \frac{Z_s \cos\varphi \cos\beta_s}{V \cos(\varphi + \beta_s)\cos(2\varphi + \beta_s)}, \tag{10}$$

$$t_{m_3} = \frac{Z_s \cos\varphi \cos\beta_s}{V \cos(2\varphi + \beta_s)\cos(3\varphi + \beta_s)}. \tag{11}$$

The total arrival time of the diffracted multiple is therefore:

$$\begin{aligned} t_m &= \frac{Z_s \cos\varphi}{V \cos(\varphi + \beta_s)} \left(1 + \frac{\cos\beta_s}{\cos(2\varphi + \beta_s)} + \frac{\cos\beta_s \cos(2\varphi + \beta_s)}{\cos(2\varphi + \beta_s)\cos(3\varphi + \beta_s)}\right) + \frac{z_d}{V \cos\beta_r} \\ &= \frac{2Z_s}{V} \frac{\cos\varphi}{\cos(\beta_s + 3\varphi)} + \frac{z_d}{V \cos\beta_r} \\ &= \frac{2(Z_D - h_D \sin\varphi)\cos\varphi}{\cos(\beta_s + 3\varphi)} + \frac{z_d}{V \cos\beta_r}, \end{aligned} \tag{12}$$

where $\tan\beta_r = \frac{m_D + h_D - x_d}{zd}$ and β_r is the emergence angle of the diffracted multiple with respect to the vertical. Figure 7 compares the moveout of the diffracted multiple with that of the water-bottom multiple. Obviously, the apex of the diffracted multiple is not at zero offset.

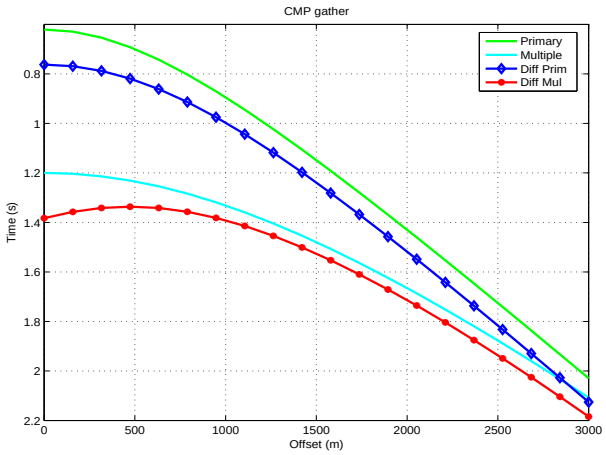

Figure 7: Moveout curves of primary, water-bottom multiple, diffraction and diffracted multiple from a dipping interface on a CMP gather. gabriel2-moveouts3 [CR]

WATER-BOTTOM MULTIPLE IN IMAGE SPACE

Given the kinematic equivalence between the water-bottom multiple and a primary from a reflector dipping at twice the dip angle, we can express the image space coordinates of the water-bottom multiple in terms of the data space coordinates by solving the system of equations presented by Fomel and Prucha (1999):

$$t_m = \frac{2\hat{Z}_\xi}{V}\frac{\cos\hat{\varphi}\cos\hat{\gamma}}{\cos^2\hat{\varphi}-\sin^2\hat{\gamma}}, \tag{13}$$

$$h_D = \hat{Z}_\xi\frac{\sin\hat{\gamma}\cos\hat{\gamma}}{\cos^2\hat{\varphi}-\sin^2\hat{\gamma}}, \tag{14}$$

$$m_D = \hat{m}_\xi + \hat{Z}_\xi\frac{\sin\hat{\varphi}\cos\hat{\varphi}}{\cos^2\hat{\varphi}-\sin^2\hat{\gamma}}, \tag{15}$$

where $(\hat{X}_\xi, \hat{m}_\xi, \hat{\gamma})$ are the image space coordinates of the primary that is kinematically equivalent to the first order water-bottom multiple as mentioned n the previous section and $\hat{\varphi} = 2\varphi$. The formal solution of these equations, for the image space coordinates is:

$$\sin\hat{\gamma} = \frac{2h_D\cos 2\varphi}{Vt_m} \longrightarrow \tan\hat{\gamma} = \frac{2h_D\cos 2\varphi}{\sqrt{V^2t_m^2-4h_D^2\cos^2 2\varphi}}, \tag{16}$$

$$\hat{Z}_\xi = \frac{\cos(2\varphi)(V^2t_m^2-4h_D^2)}{2\sqrt{V^2t_m^2-4h_D^2\cos^2(2\varphi)}}, \tag{17}$$

$$\hat{m}_\xi = m_D - \frac{V^2t_m^2\sin(2\varphi)}{2\sqrt{V^2t_m^2-4h_D^2\cos^2\varphi}}. \tag{18}$$

These equations allow the computation of the impulse response of the water-bottom multiples in image space as a function of the aperture angle. More importantly, they are the starting point for understanding the kinematics of the data in 3D ADCIGs (Tisserant and Biondi, 2004), still a subject of research.

2D SYNTHETIC DATA EXAMPLE

To illustrate the migration of the multiples, I created a simple 2D synthetic model consisting of a water-bottom reflector dipping at 15 degrees. A diffractor sits on top of this reflector at a horizontal coordinate of 5600 m. The coordinate origin is the point at which the dipping reflector intercepts the surface. Two hundred CMP gathers were generated with 100 traces in an offset range from 0 to 3000 m. The first CMP corresponds to a horizontal position of 5000 m and the CMP interval is 10 m. Four events were simulated: primary reflection, water-bottom reflection, diffraction and diffracted multiple using the traveltime equations presented before. I used a Ricker wavelet with peak frequency of 20 Hz. Figure 8 shows the zero

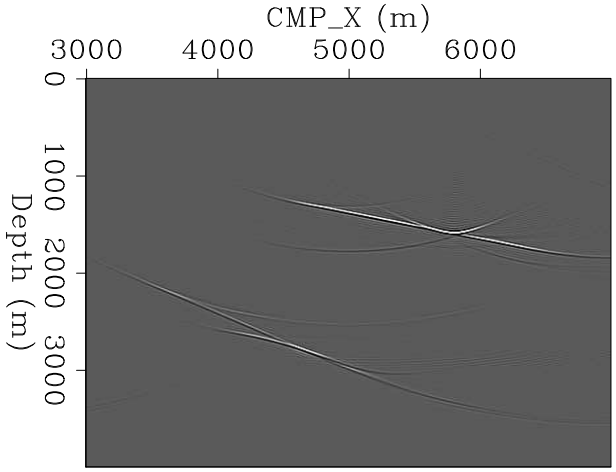

Figure 8: Zero subsurface-offset section extracted from the image obtained by migrating the data with a two constant-velocity layer model: 1500 m/s above the reflector and 2800 m/s below the reflector. gabriel2-zsoff_mig_all [CR]

subsurface offset section extracted form the image data migrated with a velocity model that consists of two constant velocity layers: 1500 m/s above the reflector and 2800 m/s below the reflector. Two reference velocities were used for the migration at each depth step. As expected, the water-bottom (primary) reflector and the diffraction are properly imaged since they were migrated with a velocity close to the true velocity. The water-bottom multiple and the diffracted multiple, on the other hand, have both been migrated. This can be seen more clearly in Figure 9, which shows four subsurface-offset common image gathers at four different horizontal locations: (a) CMP_X=6280 m, a primary location; (b) CMP_X=5800 m, diffractor location; (c) CMP_X=4600 m, a diffracted multiple location; and (d) CMP_X=3600 m, a water-bottom multiple location. The primary and the diffraction are well focused at zero subsurface offset, but not the multiples, since they were migrated with the wrong velocity.

There is, however, an important difference between the image of the water-bottom multiple and that of the diffracted multiple. This can be seen in Figure 10 that shows the zero-subsurface offset section but for the image obtained by migrating thye data with constant water velocity (1500 m/s). The primary and the diffractor are both perfectly imaged since they were migrated with the exact velocity. The water-bottom multiple is also imaged perfectly as a primary with twice the dip of the real primary. The diffracted multiple, on the other hand, is still poorly imaged and does not show as a diffractor at all, since its kinematics do not match those of a primary reflection as explained before. Figure 11 shows the same image gathers as those in Figure 9. Notice the good focusing of the water-bottom multiple. Since the “natural” prestack

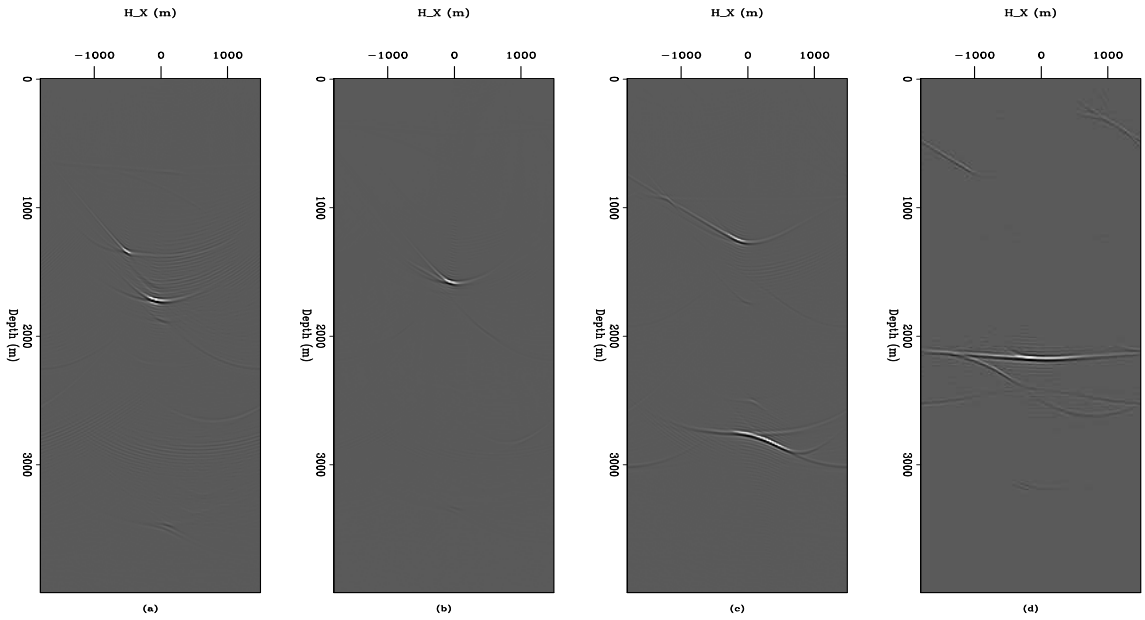

Figure 9: Subsurface-offset common-image gathers extracted form the image obtained by migrating the data with a two constant-velocity layer model. (a) at primary location (CMP_X=6280 m). (b) at the location of the diffractor (CMP_X=5800 m). (c) at a diffracted multiple location (CMP_X=4600 m) and (d) at a water-bottom multiple location (CMP_X=3600 m). gabriel2-cigs1_all [CR]

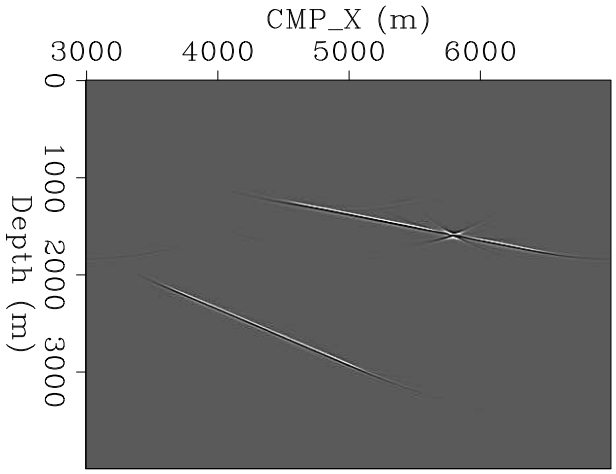

Figure 10: Zero subsurface-offset section extracted from the image obtained by migrating the data with constant water velocity. gabriel2-zsoff_mig_all_const [CR]

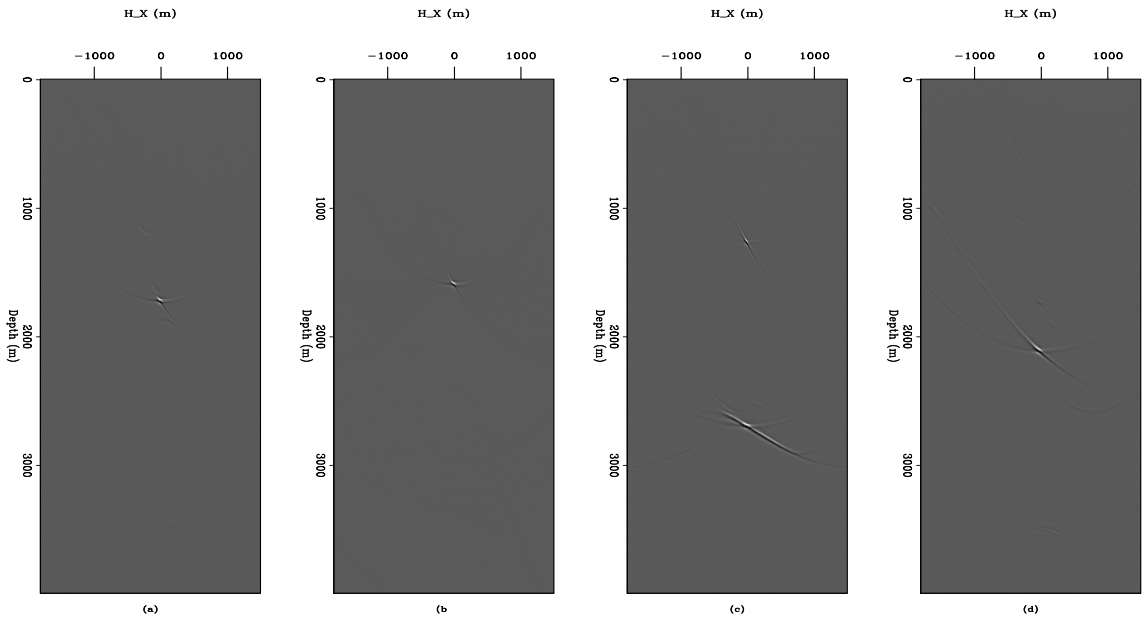

Figure 11: Subsurface-offset common image gathers extracted from the image obtained by migrating the data with constant water velocity. (a) at a primary location (CMP_X=6280 m). (b) at the location of the diffractor (CMP_X=5800 m). (c) at a diffracted multiple location (CMP_X=4600 m) and (d) at a water-bottom multiple location (CMP_X=3600 m). gabriel2-cigs1_all_const [CR]

domain of data migrated with wave-equation migration for velocity analysis is the aperture angle rather than the subsurface offset, it is worth looking at the results of the migration in this domain. Figure 12 shows angle-domain common-image gathers extracted from the image obtained by migrating the data with the two-velocity layer model at the same spatial locations as in Figure 9. The primary shows a good coverage of aperture angles. The diffraction samples even more aperture angles, since it is not restricted by Snell's law whereas the water-bottom multiple shows the characteristic overmigration. The diffracted multiple shows the expected, complicated apex-shifted moveout.

Finally, Figure 13 shows the angle-domain common-image gathers at the same spatial locations as in Figure 12 but corresponding to the data migrated with constant velocity. Notice how the moveout of then water-bottom multiple is flat like that of the primary but its range of aperture angles is much smaller as is intuitively obvious. The diffracted multiple shows focusing at its apex, located at an aperture angle of about 15 degrees.

CONCLUSIONS

I have demonstrated with a simple synthetic dataset that water-bottom multiples from a dipping interface behave as primaries generated by a reflector with twice the dip at twice the perpendicular depth at the CMP location. Therefore they can be perfectly migrated if the mi-

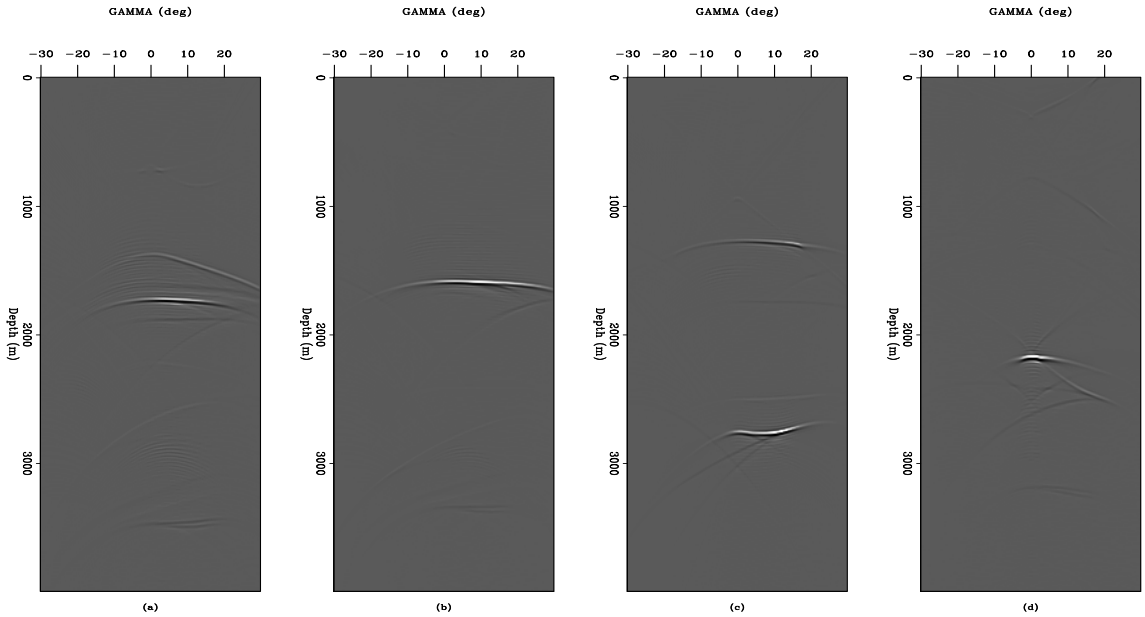

Figure 12: Angle domain common image gathers extracted from the image obtained by migrating the data with a two constant-velocity layer model. (a) at a primary location (CMP_X=6280 m). (b) at the location of the diffractor (CMP_X=5800 m). (c) at a diffracted multiple location (CMP_X=4600 m) and (d) at a water-bottom multiple location (CMP_X=3600 m). gabriel2-adcigs1_all [CR]

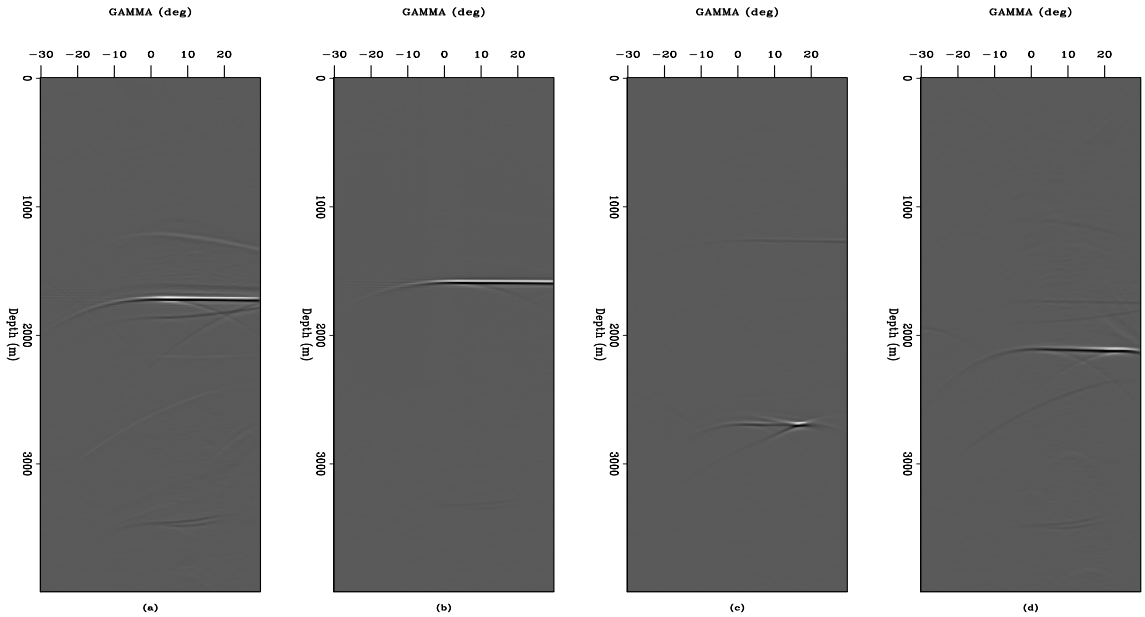

Figure 13: Angle domain common image gathers extracted from the image obtained by migrating the data with constant water velocity. (a) at a primary location (CMP_X=6280 m). (b) at the location of the diffractor (CMP_X=5800 m). (c) at a diffracted multiple location (CMP_X=4600 m) and (d) at a water-bottom multiple location (CMP_X=3600 m). gabriel2-adcigs1_all_const [CR]

gration is done with the water velocity. The diffracted multiples, on the other hand, cannot be perfectly migrated because they do not correspond to an equivalent primary. Understanding how the multiples behave after migration, specially in 3D, is very important for the ultimate goal of attenuating the multiples in image space.

REFERENCES

Alvarez, G., Biondi, B., and Guitton, A., 2004, Attenuation of diffracted multiples in angle-domain common-image gathers:, *in* 74th Ann. Internat. Mtg. Soc. of Expl. Geophys., 1301–1304.

Biondi, B., and Symes, W., 2004, Angle-domain common-image gathers for migration velocity analysis by wavefield-continuation imaging: Geophysics, **69**, no. 5, 1283–1298.

Fomel, S., and Prucha, M., 1999, Angle-gather time migration: SEP–**100**, 141–150.

Hampson, D., 1986, Inverse velocity stacking for multiple elimination:, *in* 56th Ann. Internat. Mtg. Soc. of Expl. Geophys., Session:S6.7.

Hargreaves, N., and Wombell, R., 2004, Multiple diffractions and coherent noise in marine seismic data:, *in* 74th Ann. Internat. Mtg. Soc. of Expl. Geophys., 1325–1328.

Sava, P., and Guitton, A., 2003, Multiple attenuation in the image space: SEP–**113**, 31–44.

Tisserant, T., and Biondi, B., 2004, Residual move-out analysis with 3d angle-domain common-image gathers: 74th Ann. Internat. Mtg., Soc. of Expl. Geophys., Expanded Abstracts, 2391–2394.

Verschuur, D., and Berkhout, A., 1997, Estimation of multiple scattering by iterative inversion, part ii: practical aspects and examples: Geophysics, **62**, no. 5, 1596–1611.

Verschuur, D., Berkhout, A., and Wapenaar, C., 1992, Adaptive surface-related multiple elimination: Geophysics, **57**, no. 9, 1166–1177.